Available online at www.sciencedirect.com
SCIENCE DIRECT®
Journal of Magnetic Resonance 168 (2004) 288–295
JMR Journal of Magnetic Resonance
www.elsevier.com/locate/jmr

Wavelet-based ultra-high compression of multidimensional NMR data sets☆

J. Carlos Cobas,[a,*] Pablo G. Tahoces,[b] Manuel Martin-Pastor,[a] Mónica Penedo,[c] and F. Javier Sardina[a]

[a] *Laboratorio Integral de Dinámica e Estructura de Biomoléculas José R. Carracido, Unidade de Resonancia Magnética, Edificio Cactus, RIAIDT, Universidade de Santiago de Compostela, 15782 Santiago de Compostela, Spain*
[b] *Departamento de Electrónica e Computación, Universidade de Santiago de Compostela, 15782 Santiago de Compostela, Spain*
[c] *Laboratorio de Imagen Médica, Unidad de Medicina Experimental, Hospital General Universitario Gregorio, Marañón, 28007 Madrid, Spain*

Received 18 November 2003; revised 10 February 2004
Available online 9 April 2004

Abstract

The application of a lossy data compression algorithm based on wavelet transform to 2D NMR spectra is presented. We show that this algorithm affords rapid and extreme compression ratios (e.g., 800:1), providing high quality reconstructed 2D spectra. The algorithm was evaluated to ensure that qualitative and quantitative information are retained in the compressed NMR spectra. Whilst the maximum compression ratio that can be achieved depends on the number of signals and on the difference between the most and the least intense peaks (dynamic range), a compression ratio of 80:1 is affordable even for the challenging case of homonuclear 2D experiments of large biomolecules.

Keywords: NMR; Wavelet; Data compression; Quantitative NMR

1. Introduction

High resolution multidimensional NMR spectroscopy has developed into a powerful method for the determination of the 3D structure of biological macromolecules [1,2]. Even though the technical advances in computer hardware and efficient algorithms have helped to make the handling of multidimensional data a routine task, this is possible only with higher storage capacities of the instruments computers. A typical 2D experiment could be as large as 64 Mb whereas the final size of a processed 4D spectrum reaches easily the gigabyte range [3] resulting in a considerable burden on the data storage and backup systems and low processing efficiency. Furthermore, these data must be transmitted and stored on computer networks. It is clear that advances in technology for transmission or storage are not sufficient to solve this problem. These considerations clearly raise the issue of efficient data compression.

Commonly available data compression algorithms such as gzip (Open software Foundation, Cambridge, MA), compress (Digital unix 4.0, Compaq Computer, Houston, TX), offer lossless compression ratios of as much as 6:1. To significantly affect transmission and storage costs, lossy compression methods (i.e., some information is lost in the compression process) are required, always taking into consideration that the loss must not affect either the integrity of the chemical information, i.e., all the positions of the NMR signals must be maintained without introduction of misleading artifacts, or the quantitative information of each NMR signal. In particular, the relative intensity or integral of every single signal in the spectrum respect to the rest must be retained. In addition, compression algorithms should be also valid for NMR intensity-modulated, serial experiments such as NOE, quantitative scalar coupling

☆ Supplementary data associated with this article can be found, in the online version, at doi:10.1016/j.jmr.2004.03.016.

* Corresponding author. Fax: +34-981-547077.
E-mail address: qocarlos@usc.es (J.C. Cobas).

1090-7807/$ - see front matter © 2004 Elsevier Inc. All rights reserved.
doi:10.1016/j.jmr.2004.03.016

[4–6], quantitative residual dipolar coupling [7,8], relaxation [9], and cross-correlation measurements [10].

Compression algorithms based on wavelet transform (WT) have been shown to be a very effective method of data compression. Their application to NMR spectra should be straight forward because NMR data are considerably resistant to the random distortions (noise) generated by these algorithms, which only causes an homogeneous reduction of the signal to noise level of the entire spectrum. At present, the only studies on the application of WT to the compression of high resolution NMR spectra have been limited to 1D spectra [11,12]. However, compared to the 1D method, 2D NMR data compression affords much greater compression ratios and it is where an efficient compression scheme makes practical sense anyway.

In the following, we present a fast 2D wavelet-based compression algorithm, that is generally applicable to 2D NMR data sets. We have tested this compression methodology with some examples of 2D spectra focusing on keeping the NMR signal information intact either on cases of qualitative purposes of signal assignment or on quantitative analysis as commonly required for solution structure calculations derived from nuclear Overhauser effects.

2. Theory

2.1. The wavelet transform

In this section a brief background on wavelet analysis is introduced. General principles and further details of wavelet theory are explained in [13]. The wavelet transform decomposes a signal f over wavelet functions obtained as translations u and dilations s of a mother wavelet function ψ of zero average

$$Wf(u,s) = \int_{-\infty}^{+\infty} f(t)\frac{1}{\sqrt{s}}\psi^*\left(\frac{t-u}{s}\right)\mathrm{d}t. \tag{1}$$

Shifting the translation u and scale s parameters, the wavelet transform, unlike the Fourier transform, provides a time-frequency representation of the signal. That powerful characteristic led to the WT to become a technique used for non-stationary signals in several applications, including biomedicine [14]. Additionally, sampling the translation and scale parameters as $u = 2^j n$ and $s = 2^j$, it is possible to construct a discrete orthogonal wavelet basis holding the signal details necessary to obtain a finer resolution representation of the signal, which is related with a multiresolution representation.

In a multiresolution approximation, approaches of a signal at different resolutions are determined with a discrete orthogonal basis obtained as dilations and translations of a scaling function ϕ. This multiresolution representation is completely specified by a discrete conjugate mirror filter h. It has been demonstrated that an orthogonal wavelet basis is constructed with a mother wavelet ψ, which is derived from ϕ and h, providing the detailed information lost when passing the signal to a coarser resolution representation. The orthogonal wavelet is designed with a conjugate mirror filter g given by

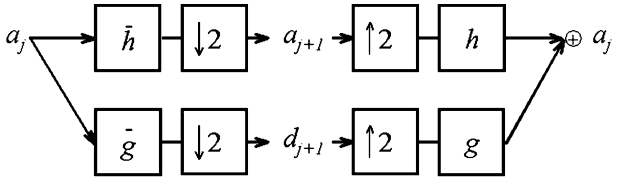

Fig. 1. Fast implementation of the 1D wavelet transform: decomposition of a_j is computed with a cascade of filterings followed by a factor 2 downsampling ($\downarrow 2$); reconstruction of a_j is done by inserting zeros between samples of a_{j+1} and d_{j+1}, filtering and adding up the output.

$$g[n] = (-1)^{1-n}h[1-n]. \tag{2}$$

A signal f at a scale 2^j is then represented in a coarse resolution as

$$f = \sum_{n=-\infty}^{+\infty} a_{j+1}[n]\phi_{j+1,n} + \sum_{n=-\infty}^{+\infty} d_{j+1}[n]\psi_{j+1,n}, \tag{3}$$

where $a_{j+1}[n] = \langle f, \phi_{j+1,n}\rangle$ and $d_{j+1}[n] = \langle f, \psi_{j+1,n}\rangle$ are the approximation coefficients and the wavelet coefficients of f at a coarse resolution, respectively. The fast implementation of the discrete wavelet transform is computed with a filter bank, which decomposes the signal with these conjugate mirror filters h and g, respectively, low and high pass filters, and subsamples the output by 2 (Fig. 1). Extension to multiple dimensions is easily obtained with separable wavelet filters, which extracts signal details at different scales and orientations, applying conjugate mirror filters along each dimension. An schematic diagram of the wavelet decomposition of an image is shown in Fig. 2.

In a wavelet-based lossy compression method, the original image is first transformed and, once in the wavelet domain, coefficients are quantized (represented with a less number of bits, which incurs in a loss of information) and entropy coded (coded with the minimum number of bits required), obtaining a compressed file. The decompression procedure reverts all this steps obtaining the reconstructed image, which is not the exact original image due to the quantization step. Further performance improvement is obtained when combined quantization and coding strategies, designed to add in characteristics of the wavelet decomposition, were used in the compression process, e.g., the set partitioning in hierarchical trees (SPIHT)[1] algorithm.

[1] *Abbreviations used:* β-CD, β-cyclodextrin; FGF, fibroblast growth factor; PSNR, peak signal-to-noise ratio; SPIHT, set partitioning in hierarchical trees.

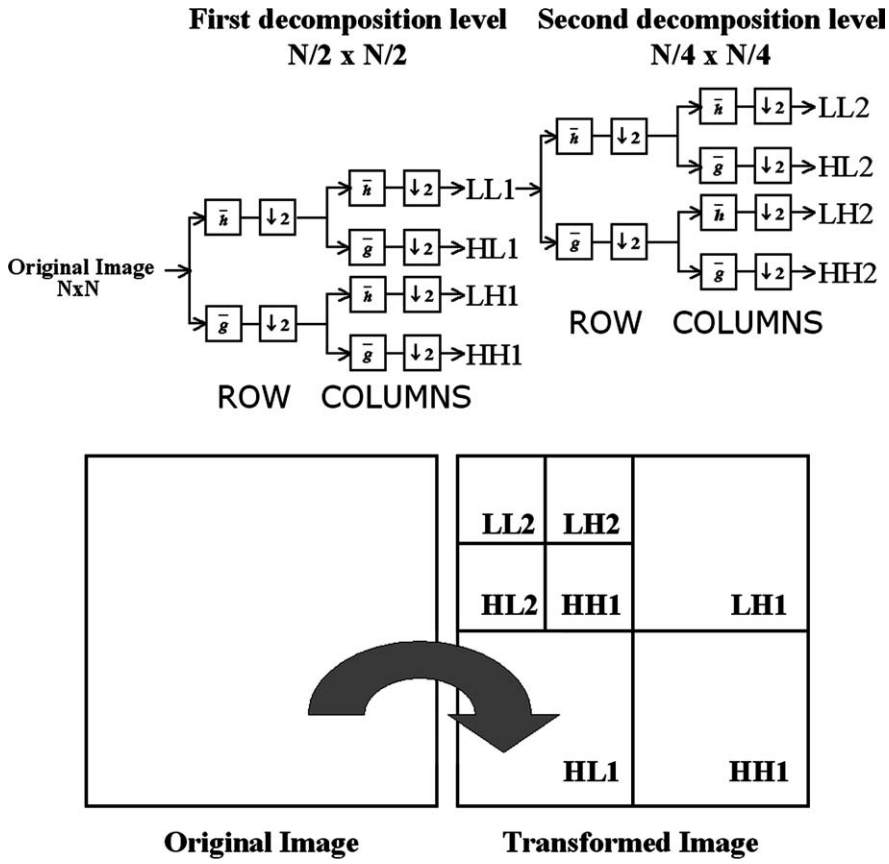

Fig. 2. Schematic diagram of the 2D dyadic wavelet decomposition. In the original image, each row is first filtered and subsampled by 2, then, each column is filtered and subsampled by 2. Four subimages are obtained, called wavelet subbands, referred to as HL, LH, HH: high frequency subbands, and LL: low frequency subband. The LL subband is again filtered and subsampled to obtain four more subimages. This process can be repeated until the desired decomposition level.

In this work, a four-level decomposition of the images was obtained with the 2D discrete wavelet transform using 9/7 biorthogonal wavelet filters. Numerical studies have shown that the 9/7 biorthogonal filters provide the best distortion rate performance for wavelet-based image compression [13,15,16].

2.2. SPIHT coding algorithm

Set partitioning in hierarchical trees (SPIHT) is an efficient wavelet-based coding algorithm developed by Said and Pearlman [17]. In terms of image compression performance it is the state-of-the-art. This coding method is an extension and an improvement over the embedded zerotree wavelets (EZW) algorithm developed by Shapiro [18]. The SPIHT method takes advantage of the spatial self-similarity across subbands inherent in the image wavelet transform, i.e., there are wavelet coefficients in different subbands of the transformed image that represent the same spatial localization in the original image (see Appendix in the supplementary material). Recent studies have successfully applied SPIHT to lossy compression of medical images [19–21]. Software implementation of the SPIHT coding algorithm used in this study was developed in C language. Compression process duration was 6 s per image when an UltraSPARC workstation (Sun Microsystems, Santa Clara, CA, USA) with a processor of 450 MHz was used to run the program over an 8 Mb spectrum.

2.3. Measures of performance

A compression algorithm can be evaluated by using different measures: distortion introduced in the process, memory requirements for method execution, relative complexity and speed of the algorithm, compression ratio, etc. A common way to report compression performance is to provide the average number of bits required to represent a single sample of the compressed image. This is generally referred to as the compression rate, and bits per pixel (bpp) is used as the unit of measure. For instance, given a 2D spectrum of 1024×1024 pixels (1,048,576 pixels), where 16 bits represent each pixel, the total amount of bits necessary to store the spectrum is 16,777,216. Suppose that after compression the resulting amount of bits is 4,194,304. This result is equivalent to having a spectrum of 1024×1024 pixels with only 4 bits representing each

pixel. It would be said that the compression rate is 4 bpp or, equivalently, the compression ratio is 4:1, where

$$\text{Compression ratio} = \frac{\text{rate of the original spectra}}{\text{rate of the compressed spectra}}. \quad (4)$$

Another important issue is to establish the quality of the compressed image, i.e., the distortion introduced in the compression process. As the compression ratio increases, the quality of the resulting image is degraded. Therefore, a parameter for measuring the degree of distortion introduced is needed. In our paper, the reconstruction quality of the method was evaluated by means of the peak signal-to-noise ratio (PSNR), which is often measured in a logarithmic scale

$$\text{PSNR } ([\text{dB}]) = 10\log_{10}\left(\frac{A^2}{\text{MSE}}\right), \quad (5)$$

where A is the peak amplitude of the original image, and MSE is the mean squared-error between the original and the reconstructed spectra

$$\text{MSE} = \frac{1}{N}\sum_{n=1}^{N}(x_{ij}(n) - \hat{x}_{ij}(n))^2, \quad (6)$$

with $x_{ij}(n)$ and $\hat{x}_{ij}(n)$ representing the original and the reconstructed spectra, respectively, and N representing the number of pixels of the spectra.

3. Results and discussion

Lossy compression performance of the wavelet-based coding method was evaluated for several 2D NMR examples representative of different types of spectra. The 2D HMQC-COSY (magnitude mode), 2D TOCSY (phase sensitive), and 2D HSQC (phase sensitive) experiments, were used to evaluate the SPIHT algorithm for the compression of qualitative information (signal assignment). On the other hand, a series of 2D NOESY experiments (phase sensitive) were chosen to evaluate the SPIHT algorithm for the compression of quantitative NMR information. The usually rather small NOE signal intensity suppose a very demanding test for the compression algorithm. The results of the evaluation of the different experiments by means of the PSNR (Eq. (5)) of the different spectra are given in Table 1 and Fig. 3.

The results of the 2D HMQC-COSY spectrum of a sample of β-cyclodextrin (β-CD), clearly show the ability of the SPIHT compression algorithm to maintain integrity of the NMR assignment. Even though at a compression ratio of 800:1 there was a slight decrease in the PSNR (Fig. 3), the comparison between the original 2D spectrum and the one reconstructed at this high compression factor showed that they were almost identical (Fig. 4).

To evaluate the performance of the method in situations when the number of signals is higher, we chose the 2D TOCSY and 2D ^{15}N-HSQC spectrums of the human acidic fibroblast growth factor (FGF) protein [22]. For the former spectrum it was found that compression ratios of 800:1 and 320:1 result in a loss of the least intense peaks, whereas at 80:1 all the signals were retained. In the case of the ^{15}N-HSQC spectrum (Fig. 5), the best compromise between compression and spectral quality was found when a compression ratio of 160:1 was used; it is clear from Figs. 5A and C that both spectra were almost identical. In this example, the original 4 Mb file was reduced to just 25.6 Kb.

To check the limits for which the lossy SPIHT compression is able to ensure that the absolute intensities of the signals (i.e., integral volumes) in the decompressed spectrum match those in the raw, original uncompressed spectrum, a quantitative test was performed. Thus, a series of 2D NOESY experiments of the β-CD sample were acquired under the same conditions but varying the mixing time between 50 and 500 ms in different experiments. The five well-resolved NOEs from H-1 to protons H-2, H-3, H-4, H-5, and H-6 in the β-CD were quantified (see Section 5) to determine NOE cross-relaxation rates at different compression ratios, detailed in Table 2. NOE cross-relaxation rate is a very sensitive parameter to check for potential artifacts or biasing occurring to the peak integrals as a result of the use of the compression algorithm. Table 2 shows that when the data was compressed at a very high ratio of 800:1, the values of H1–H5 and H1–H6 differed significantly from

Table 1
PSNR (in decibels) at various compression ratios for all the spectra analyzed

Ratio	Rate (bbp)	HMQC-COSY	NOESY							TOCSY	HSQC
			50 ms	100 ms	150 ms	200 ms	350 ms	400 ms	500 ms		
16:1	1	81.61	84.56	84.7	84.79	85.29	85.58	85.56	85.85	40.56	74.15
20:1	0.8	79.88	82.28	82.41	82.49	82.91	83.17	83.21	83.53	40.26	72.07
26.7:1	0.6	78.42	79.97	80.08	80.16	80.51	80.72	80.82	81.18	38.67	69.69
40:1	0.4	76.79	77.89	77.98	78.05	78.36	78.56	78.65	78.87	38.3	66.54
80:1	0.2	74.59	74.77	74.96	75.1	75.55	75.76	75.93	76.3	36.03	62.32
160:1	0.1	72.95	70.14	70.38	70.63	71.32	71.54	72.01	72.69	35.43	59.3
320:1	0.05	71.87	62.96	63.5	63.81	64.42	64.81	65.65	66.34	32.91	57.25
800:1	0.02	70.92	51.81	52	33.09	52.35	36.07	54.05	55.14	29.45	54.77

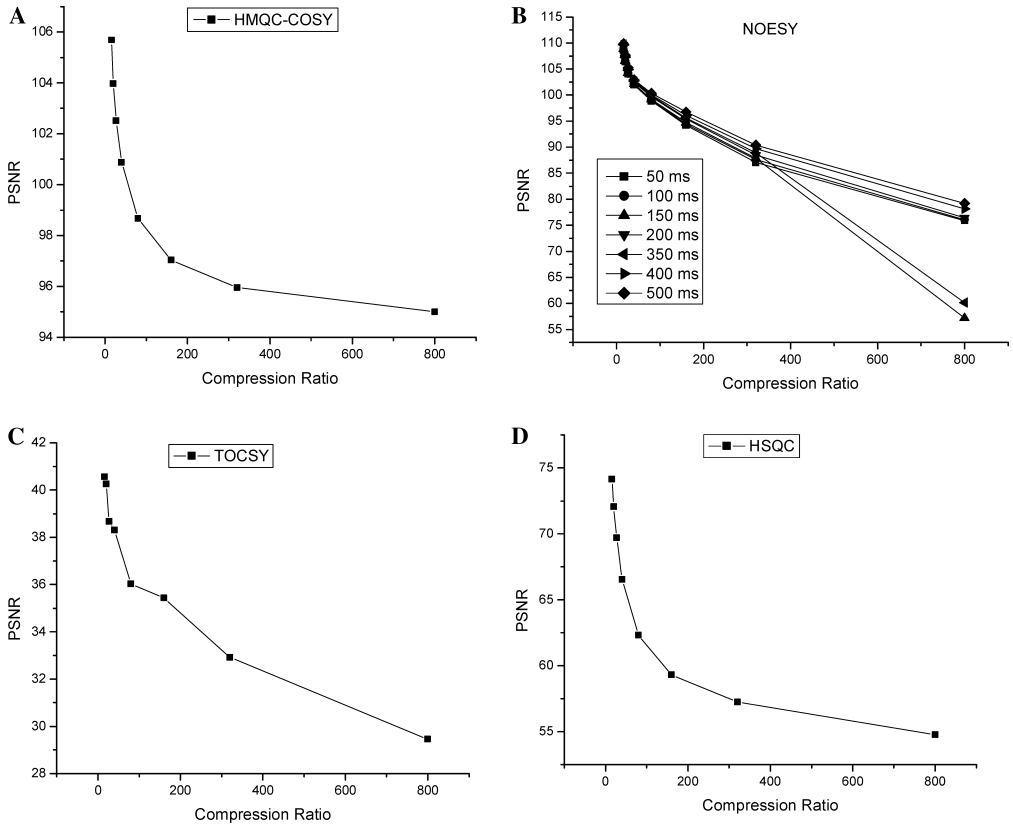

Fig. 3. Plots of PSNR vs. compression ratio for the spectra (A) 2D HMQC-COSY of β-CD, (B) 2D NOESY of β-CD, (C) 2D TOCSY of FGF protein, and (D) 2D ^{15}N-HSQC of FGF protein.

the values obtained from the uncompressed spectrum. A close look at the absolute integral values in the compressed spectra shows that SPIHT tends to scale down all the integrals in the spectrum by a similar factor. Eventually, at a very high compression ratio the lowest intense signals (e.g., the two very small NOEs at the shortest mixing times) were almost reduced to the noise level, causing the erroneous values observed in the fit for the cross-relaxation. This effect was also observed in the significant diminution of the PSNR values (see Fig. 3B). This problem did not occur at the compression ratios of 320:1 and 80:1 (Table 2), for which the results were virtually similar to the original spectrum and the small differences basically reflected the proper signal integration accuracy. At these two compression ratios, the straight forward calculation from the determined NOE cross-relaxation rates to proton–proton distance (see Section 5) gave deviations below 0.3% in the determined distances a range of error that is by far below the accuracy of the NMR NOE methods (data not shown).

4. Conclusions

We have shown that high compression rates (up to 800:1) can be achieved with the wavelet-based algorithm presented in this work. The maximum compression ratio affordable depends on the quality of the original spectrum itself (signal to noise ratio), the total number of signals, and the user's needs to preserve certain small signals of interest above a certain signal to noise level.

When the number of signals in the spectrum is not too high and the signal to noise ratio of the original spectrum is high, as it usually happens in HMQC and related experiments of medium-sized organic molecules, very high compression ratios can be used without risk of losing the qualitative chemical information (e.g., the 800:1 compression ratio of Fig. 4).

When quantitative information is required or the number of signals is high, more modest levels of compression should be used instead to avoid losing the information from the less intense peaks, but even in the most unfavorable cases, such as the quantification of small NOE intensities, a compression ratio of 80:1 can be used safely.

We are confident that spectral NMR databases would benefit from this compression scheme, leading to a more efficient data handling and processing. Future work will involve the extension of the algorithm to compress 3D and 4D spectra. Considering the sparse nature of each 2D plane, it is expected that the performance of the method will be even higher. In addition, work to allow

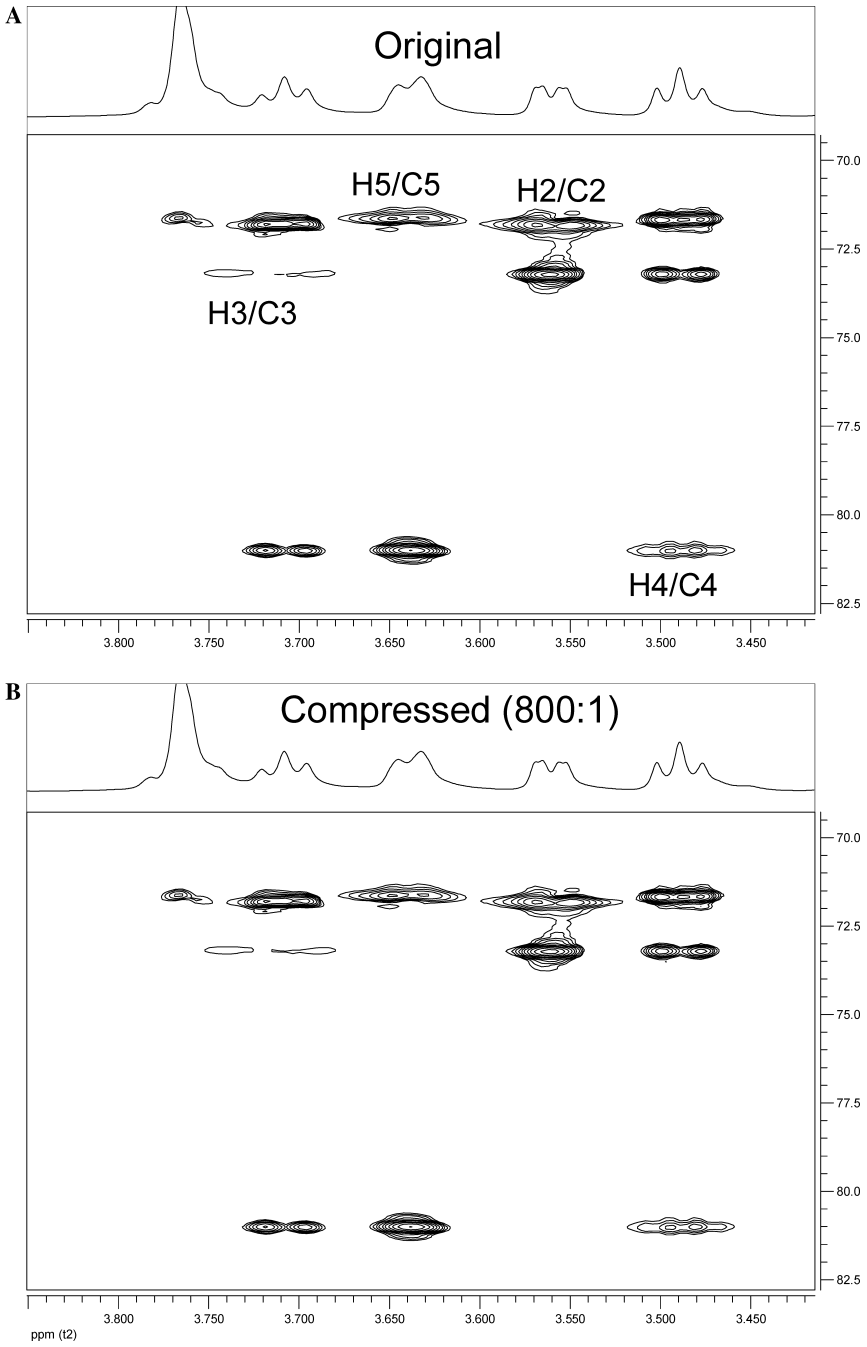

Fig. 4. 2D HQMC-COSY of β-CD, original spectrum (A) and compressed at a compression ratio of 800:1. (B) Only the spectral region of signals H2–H5 is displayed.

the automatic calculation of the best compression factor with minimum user intervention is currently in progress.

5. Experimental

5.1. Sample preparation

Fifteen milligrams of β-cyclodextrin (β-CD) (Sigma) were dissolved in 0.5 ml D_2O 99.9% (Sigma).

Two samples of 8 mg of human acidic FGF protein (^{15}N-labeled and unlabeled) were dissolved in H_2O/D_2O (90/10) with phosphate buffer.

5.2. NMR experiments

NMR experiments were acquired on a 750 MHz Varian INOVA or in a 500 MHz DRX Bruker Avance spectrometer. The spectra were processed with MestRe-C [23] software.

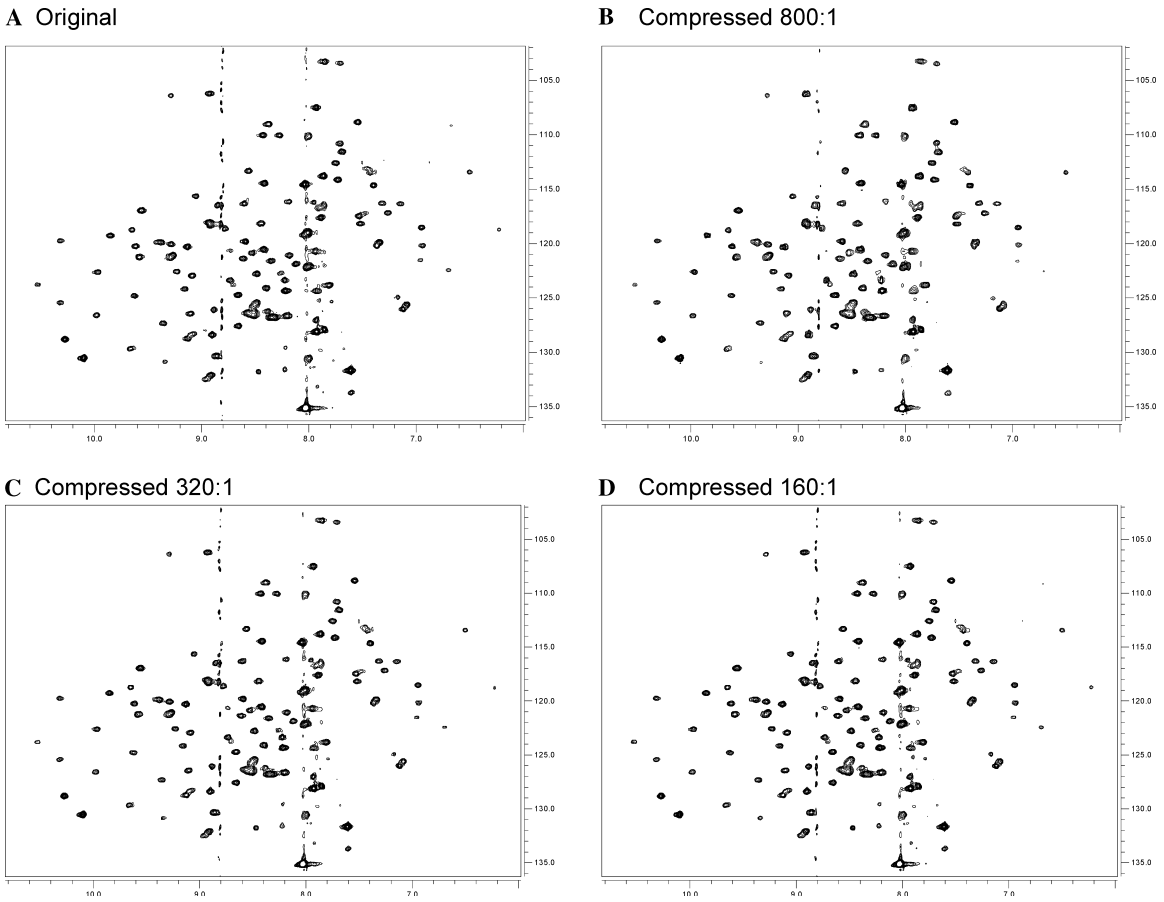

Fig. 5. 2D ^{15}N-HSQC of the FGF protein. (A) Original uncompressed spectrum. (B) Compressed at 800:1 ratio. (C) At 320:1 and (D) at 160:1.

Table 2
Experimental cross relaxation rates, σ_{ij}, for different proton pairs of β-CD from the analysis of 2D NOESY intensities at the different compression ratios

Proton pair	Compression ratio			
	1:1[a]	800:1	320:1	80:1
H1–H2	0.07426	0.07143	0.07412	0.07426
H1–H3	0.00881	0.00801	0.00848	0.00882
H1–H5	0.01015	0.01152[b]	0.01021	0.01019
H1–H4	0.09667	0.09623	0.09645	0.09678
H1–H6	0.01041	0.00656[b]	0.01035	0.01039
Size (kb)	2048	2.56	6.4	25.6

[a] Uncompressed spectra.
[b] These values deviate significantly.

A 2D HMQC-COSY experiment [24,25] acquired at 750 MHz was used for the unambiguous assignment of ^{1}H and ^{13}C resonances of β-CD. In this experiment COSY peaks are resolved in the ^{13}C dimension of a 2D ^{1}H/^{13}C correlation. The spectrum was acquired with 1176 complex points and 400 increments in F2 and F1, respectively. The data was Fourier transformed and processed to 2 K × 2 K data points using a 90° sine-square apodization along F2 and 0° sine-bell in F1 and displayed in magnitude mode. The final processed spectrum occupied 8 Mb.

2D WET-TOCSY experiment was acquired at 750 MHz for human acidic FGF protein (H_2O, 90%). The residual solvent signal was suppressed with a high pass filter on the time domain. The raw FID data are 2048 × 512 (hypercomplex points). In both dimensions the FID data were multiplied by a cosine square function and Fourier transformed to 2 K × 2 K. Final size is 8 Mb.

2D WET-HSQC experiment ^{15}N-labeled FGF protein sample was acquired at 500 MHz (H_2O, 90%). The raw FID data are 1024 × 256 (hypercomplex points). In both dimensions the FID data were multiplied by a cosine square function and Fourier transformed to 4096 × 512. Final size is 4 Mb.

2D NOESY experiments were acquired at 500 MHz for the β-CD sample at the following mixing times 0.05, 0.1, 0.15, 0.2, 0.35, 0.4, and 0.5 s. Each spectrum was acquired with 1024 × 256 complex points in F2 and F1, respectively. The data was Fourier transformed and processed to 1 K × 1 K data points using a 90° sine-square apodization along both dimensions. Each processed spectrum occupies 2 Mb.

5.3. NOE quantitative analysis

NOE intensities from the isolated proton resonance H1 of β-CD were analyzed at the different mixing times using the initial rate approximation [26]. In this approach the interproton dipolar cross relaxation rate of a given proton pair is determined from the slope of the initial part of the corresponding NOE build-up curve. In the case of β-CD all the different NOE considered were found to behave fairly linear in the range of mixing times explored. Thus, a linear fit of a given NOE cross peak intensity versus mixing time provided the cross relaxation rate. The conversion from cross relaxation rate to proton–proton distance was done according to the distance reference method [26] by using the following equation (Eq. (7)):

$$r_{ij} = r_{\mathrm{ref}} \cdot \sqrt[6]{\frac{\sigma_{ref}}{\sigma_{ij}}}. \tag{7}$$

In this equation r_{ij} and σ_{ij} are the unknown distance and the measured cross relaxation rate of any given pair of protons i and j, respectively, while r_{ref} and σ_{ref} are the analogue values of a proton pair which is used as reference, for which r_{ref} is a priori known in the molecule. In the case of β-CD the reference distance used was the intra-sugar ring distance between the proton pair H1–H2 which is 2.34 Å in the crystal structure of β-CD [27].

Acknowledgments

Financial support from the CICYT (Grant BQU2002-01368) and the Xunta de Galicia (Grant PGIDIT03PXIC20910PN) is gratefully acknowledged. We thank Prof. J. Jiménez-Barbero for providing the FGF protein.

References

[1] K. Wuthrich, NMR of Proteins and Nucleic Acids, Wiley, New York, 1986.
[2] J. Jiménez-Barbero, T. Peters, NMR Spectroscopy of Glycoconjugates, Wiley-VCH, New york, 2002.
[3] E.R.P. Zuiderweg, A.M. Petros, S.W. Fesik, E.T. Olejniczak, Four-dimensional [^{13}C, ^{1}H, ^{13}C, ^{1}H] HMQC-NOE-HMQC NMR spectroscopy: resolving tertiary NOE distance constraints in the spectra of larger proteins, J. Am. Chem. Soc. 113 (1991) 370–372.
[4] P.R. Blake, B. Lee, M.F. Summers, M.W. Adams, J.B. Park, Z.H. Zhou, A. Bax, Quantitative measurement of small through-hydrogen-bond and "through-space ^{1}H–^{113}Cd and ^{1}H–^{199}Hg *J* couplings in metal-substituted rubredoxin from *Pyrococcus furiosus*, J. Biomol. NMR 2 (1992) 527–533.
[5] G. Vuister, A. Bax, Quantitative *J* correlation: a new approach for measuring homonuclear three-bond $J(H^{N}H^{\alpha})$ coupling constants in ^{15}N-enriched proteins, J. Am. Chem. Soc. 115 (1993) 7772–7777.
[6] N. Tjandra, A. Bax, Measurement of dipolar contributions to 1JCH splittings from magnetic field dependence of *J* modulation in two-dimensional NMR spectra, J. Magn. Reson. 124 (1997) 512–515.
[7] F. Tian, P.J. Bolon, J.H. Prestegard, Intensity based measurement of homonuclear residual dipolar couplings from CT-COSY, J. Am. Chem. Soc. 121 (1999) 7712–7713.
[8] Z. Wu, A. Bax, Measurement of homonuclear proton couplings based on cross-peak nulling in CT-COSY, J. Magn. Reson. 151 (2001) 242–252.
[9] T. Yamazaki, R. Muhandiram, L.E. Kay, NMR experiments for the measurement of carbon relaxation properties in highly enriched, uniformly ^{13}C, ^{15}N-labeled proteins: application to 13Cα carbons, J. Am. Chem. Soc. 116 (1994) 8266–8278.
[10] B. Reif, M. Henning, C. Griesinger, Direct measurement of angles between bond vectors in high-resolution NMR, Science 276 (1997) 1230–1233.
[11] X.G. Shao, H. Gu, W.S. Cai, Z.X. Pan, Studies on data compression, of 1-D NMR Spectra using wavelet transform, Spectrosc. Anal. 19 (1999) 139–141.
[12] X.G. Shao, A.K.M. Leung, F.T. Chau, Wavelet: a new trend in chemistry, Acc. Chem. Res. 36 (2003) 276–283.
[13] S.G. Mallat, A Wavelet Tour of Signal Processing, Academic Press, San Diego, 1999.
[14] M. Unser, A. Aldroubi, A review of wavelets in biomedical applications, Proc. IEEE 84 (1996) 626–638.
[15] M. Antonini, M. Barlaud, P. Mathieu, I. Daubechies, Image coding using wavelet transform, IEEE Trans. Image Process. 1 (1992) 205–220.
[16] J. Villasenor, B. Belzer, J. Liao, Wavelet filter evaluation for image compression, IEEE Trans. Image Process. 4 (1995) 1053–1060.
[17] A. Said, W. Pearlman, A new fast and efficient image codec based on set partitioning in hierarchical trees, IEEE Trans. Circuits Syst. Video Technol. 6 (1996) 243–250.
[18] J.M. Shapiro, Embedded image coding using zerotrees of wavelet coefficients, IEEE Trans. Signal Process. 41 (1993) 3445–3462.
[19] V. Savcenko, B.J. Erickson, P.M. Palisson, K.R. Persons, A. Manduca, T.E. Hartman, G.F. Harms, L.R. Brown, Detection of subtle abnormalities on chest radiographs after irreversible compression, Radiology 206 (1998) 609–616.
[20] S. Perlmutter, P. Cosman, R. Gray, R. Olshen, D. Ikeda, C. Adams, B.J. Betts, M. Williams, K. Perlmutter, J. Li, A. Aiyer, L. Fajardo, R. Birdwell, B. Daniel, Image quality in lossy compressed digital mammograms, Signal Process. 59 (1997) 189–210.
[21] M. Penedo, W.A. Pearlman, P.G. Tahoces, M. Souto, J.J. Vidal, Region-based wavelet coding methods for digital mammography, IEEE Trans. Med. Imaging 22 (2003) 1288–1296.
[22] A. Pineda-Lucena, M.A. Jiménez, J.L. Nieto, J. Santoro, M. Rico, G. Giménez-Gallego, ^{1}H-NMR assignment and solution structure of human acidic fibroblast growth factor activated by inositol hexasulfate, J. Mol. Biol. 242 (1994) 81–98.
[23] J.C. Cobas, F.J. Sardina, Nuclear magnetic resonance data processing: MestRe-C, a software package for desktop computers, Concept. Magn. Reson. A 19 (2) (2003) 80–96.
[24] L. Lerner, A. Bax, Sensitivity-enhanced two-dimensional heteronuclear relayed coherence transfer NMR spectroscopy, J. Magn. Reson. 69 (1986) 375–380.
[25] W. Willker, D. Leibfritz, R. Kerssebaum, W. Bermel, Gradient selection in inverse heteronuclear spectroscopy, Magn. Reson. Chem. 31 (1993) 287–292.
[26] D. Neuhaus, M.P. Williamson, The Nuclear Overhauser Effect in Structural and Conformational Analysis, second ed., Wiley-VCH, New York, 2000, pp. 112–113.
[27] J.M. Alexander, J.L. Clark, T.J. Brett, John J. Stezowski, Chiral discrimination in β cyclodextrin *N*-acetyl-L-phenylalanine and *N*-acetyl-D-phenylalanine complexes, PNAS 99 (2002) 5115–5120.